

Environmental Science Nano

Accepted Manuscript

This article can be cited before page numbers have been issued, to do this please use: M. K. Gari, P. Lemke, K. H. Lu, E. Laudadio, A. Henke, C. M. Green, T. Pho, K. N. Hoang, C. Murphy, R. Hamers and Z. V. Feng, *Environ. Sci.: Nano*, 2021, DOI: 10.1039/DOEN01151G.



This is an Accepted Manuscript, which has been through the Royal Society of Chemistry peer review process and has been accepted for publication.

Accepted Manuscripts are published online shortly after acceptance, before technical editing, formatting and proof reading. Using this free service, authors can make their results available to the community, in citable form, before we publish the edited article. We will replace this Accepted Manuscript with the edited and formatted Advance Article as soon as it is available.

You can find more information about Accepted Manuscripts in the [Information for Authors](#).

Please note that technical editing may introduce minor changes to the text and/or graphics, which may alter content. The journal's standard [Terms & Conditions](#) and the [Ethical guidelines](#) still apply. In no event shall the Royal Society of Chemistry be held responsible for any errors or omissions in this Accepted Manuscript or any consequences arising from the use of any information it contains.

Environmental Significance

Routine environmental nanotoxicology observations are often made without considering the dynamic transformation of the nanomaterials over time, which may lead to observations that cannot be deconstructed adequately into each variable separately. This work investigates the dynamic transform of lithium cobalt oxide (LiCoO_2) nanosheets in solutions by both abiotic reactive oxygen species (ROS) generation and Co ion release, and delineates their respective biological impacts in a model bacterium, *B. subtilis*. The observed additional changes in oxidative stress genes and DNA damages in *B. subtilis* coincide with the burst of H_2O_2 in fresh nanoparticle suspensions, which provides direct evidence to connect the abiotic ROS generated by the nanoparticles to the oxidative stress responses in organism. Therefore, the study illustrates a new approach to evaluate nanotoxicity and reveals the importance of evaluating abiotic ROS generation in complex metal oxide nanoparticles.

ARTICLE

Dynamic Aqueous Transformations of Lithium Cobalt Oxide Nanoparticle Induce Distinct Oxidative Stress Responses of *B. subtilis*

Received 00th January 20xx,
Accepted 00th January 20xx

DOI: 10.1039/x0xx00000x

Metti K. Gari^a, Paul Lemke^a, Kelly H. Lu^a, Elizabeth D. Laudadio^b, Austin H. Henke^b, Curtis M. Green^b, Thomas Pho^{a,†}, Khoi Nguyen L. Hoang^c, Catherine J. Murphy^c, Robert J. Hamers^b, Z. Vivian Feng^{a*}

Abstract: Lithium cobalt oxide (LiCoO₂), an example of nanoscale transition metal oxide and a widely commercialized cathode material in lithium ion batteries, has been shown to induce oxidative stress and generate intracellular reactive oxygen species (ROS) in model organisms. In this study, we aimed to understand the time-dependent roles of abiotic ROS generation and Co ions released in aqueous medium by LiCoO₂ NPs, and examined the induced biological responses in model bacterium, *B. subtilis* upon exposure. We found that the redox-active LiCoO₂ NPs produced abiotic ROS primarily through H₂O₂ generation when freshly suspended. Subsequently, the freshly-suspended LiCoO₂ NPs induced additional DNA breakage, and changes in expression of oxidative stress genes in *B. subtilis* that could not be accounted for by the released Co ions alone. Notably, in 48-hour old LiCoO₂ suspensions, H₂O₂ generation subsided while higher concentrations of Co ions were released. The biological responses in DNA damage and gene expression to the aged LiCoO₂ NPs recapitulated those induced by the released Co ions. Our results demonstrated oxidative stress mechanisms for bacteria exposed to LiCoO₂ NPs were mediated by the generation of distinct biotic and abiotic ROS species, which depended on the aqueous transformation state of the NPs. This study revealed the interdependent and dynamic nature of NP transformation and their biological consequences where the state of NPs resulted in distinct NP-specific mechanisms of oxidative injury. Our work highlights the need to capture the dynamic transformation of NPs that may activate the multiple routes of oxidative stress responses in cells.

Introduction

With the widespread use of nanoscale materials in a variety of fields, research into their biological and environmental impact becomes increasingly important. Several metal oxides, such as TiO₂ and ZnO, due to their applications as photocatalysts^{1,2} and in food industry and medical applications^{3,4}, have been more broadly studied for their biological and environmental impacts. As energy demand grows and fossil fuel resources dwindle, lithium-ion batteries with promising high cell potential, high gravimetric and volumetric capacity, and good cycling performance have taken the center stage recently.^{5,6} Consequently, a class of lithium intercalating complex metal oxide nanomaterials has emerged, and is produced in large quantities as battery cathodes.⁷ To date, lithium cobalt oxides, LiCoO₂, is one of the most ubiquitously used complex metal oxides – from electric vehicles to consumer microelectronic devices. A lack of economic incentives and infrastructure for recycling of these materials^{8,9}

especially calls for studies to examine the environmental and biological impact of these novel nanomaterials at the end of their life cycle and entrance into the environment.

Metal oxide nanoparticles can lead to cytotoxicity through dissolution of metal ions when placed in media, largely due to their high surface-to-volume ratios. For instance, lithium nickel manganese cobalt oxide has been shown to release toxic levels of nickel, manganese, and cobalt ions that impact bacterial respiration^{10,11} and the lifecycle of *Daphnia magna*.¹² Yet, often, the dissolved ions cannot fully recapitulate the biological impacts induced by the nanoparticles. In eukaryotic cells where nanoparticles may be internalized, cytotoxicity has been linked to nanoparticle-induced intracellular reactive oxygen species (ROS) generation and cellular oxidative stress.¹³ Metal oxide nanoparticles can induce ROS due to their reactive surfaces, semiconductor electronic properties, or through the release of redox active transition metal ions triggering biomolecule redox reactions.¹⁴ Species, such as superoxide, hydroxyl radical, and hydrogen peroxide, once formed intracellularly at levels that overwhelm the antioxidant systems, often result in oxidative stress exhibited by DNA damage or lipid peroxidation.^{14–16} The overproduction of ROS and imbalance of antioxidant defence system can lead to different diseases and cell death.¹⁷ Therefore, examining the mechanisms leading to the production of intracellular ROS and

^a Chemistry Department, Augsburg University, Minneapolis, MN 55454

^b Department of Chemistry, University of Wisconsin, Madison, WI, 53706

^c Department of Chemistry, University of Illinois at Urbana-Champaign, Urbana, IL, 61801.

† Present address: Department of Chemical Engineering, Georgia Institute of Technology, Atlanta, GA, 30332

Electronic Supplementary Information (ESI) available: [details of any supplementary information available should be included here]. See DOI: 10.1039/x0xx00000x

1 ARTICLE

2 the biological consequences has been proposed as a paradigm for
 3 NP toxicity.^{1,18}

4 Some metal oxides, especially semiconductors and photocatalysts,
 5 have been shown to spontaneously generate abiotic ROS.^{3,18–20} We
 6 have previously detected evidence for abiotic ROS produced from
 7 lithium nickel cobalt oxide suspensions as the material undergoes
 8 incongruent dissolution.²¹ The production of ROS, especially
 9 superoxide, by TiO₂ has been demonstrated both in response to UV
 10 radiation^{19,22} and in the dark.³ These findings raise the question of
 11 whether abiotic ROS can directly induce intracellular ROS and
 12 trigger oxidative stress responses in model organisms. However, to
 13 delineate the biological responses due to ROS vs. metal ions is a
 14 challenging question where few studies have attempted to answer,¹
 15 and requires a highly systematic approach.

16 The question is further complicated by the dynamic nature of both
 17 NP transformation and their biological consequences. Although
 18 studies have demonstrated the kinetics of metal ion dissolution from
 19 metal oxides,^{10,11,21,23} few have paid equal attention to monitor the
 20 time-dependent ROS generation from nanoparticles.¹ In addition,
 21 when organisms are exposed to nanomaterials for extended period
 22 of time (e.g. days), the studies often result in examining the impact
 23 from two coupled variables over time: material transformation and
 24 biological responses. Cui et al. demonstrated the dynamic oxidative
 25 stress responses from trout gill cells over 48 hrs in a series of elegant
 26 single-cell gene expression experiments where different genes were
 27 triggered at different time points upon exposure to LiCoO₂.²⁴ These
 28 findings further highlighted the needs for investigating the dynamic
 29 process of LiCoO₂ transformation and the cellular responses.

30 In this study, we monitor the dynamic transformation of LiCoO₂ in
 31 terms of Co release and abiotic ROS generation, and examine the
 32 biological impact of the transformed LiCoO₂ towards a model
 33 bacterium, *B. subtilis*. *B. subtilis* is a ubiquitous Gram-positive
 34 bacterium that plays major roles in the terrestrial carbon cycle to
 35 supply nutrients to plants, and has well-characterized genomes. In
 36 contrast to eukaryote cells where nanoparticles can be
 37 internalized,^{25,26} bacteria do not usually take up the
 38 nanoparticles.^{10,21,27,28} Therefore, using bacterial models eliminates
 39 the complication that material intracellular transformation may
 40 differ from that characterized *in situ*. By using species-specific probes
 41 and biochemical assays, we aim to detect and identify the
 42 spontaneously generated ROS in growth medium as well as
 43 intracellular ROS, and establish connections between them. In order
 44 to isolate the two time-dependent variables of material
 45 transformation and biological responses, we designed experiments
 46 to allow LiCoO₂ NP suspensions to age in the absence of bacterium
 47 for 1 hour and 48 hours, and characterized ion release and abiotic
 48 ROS generation at two different time points. We then treated *B.*
 49 *subtilis* with the 1-hr and 48-hr aged LiCoO₂ suspensions for a short
 50 duration of 30 minutes to minimize the variations in biological
 51 responses over time. We assessed oxidative stress markers, such as
 52 DNA damage and changes in gene expression in *B. subtilis* upon
 53 exposure to LiCoO₂ suspensions. Results indicate that additional
 54 oxidative stress in bacterium that cannot be fully accounted for by
 55

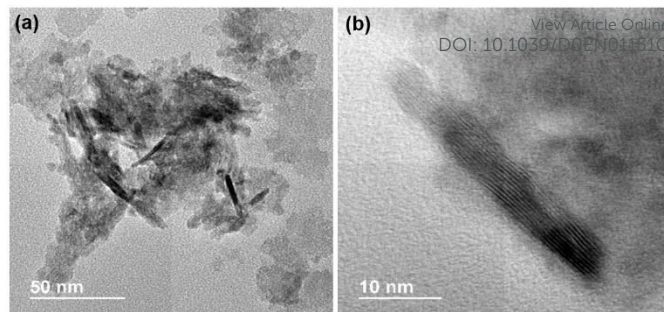


Figure 1. Transmission electron micrographs of pristine LiCoO₂ nanoparticles.

56 the Co ion released were observed in freshly suspended LiCoO₂
 57 solutions, overlapping with the burst of H₂O₂ generation in solution,
 58 which suggests that abiotic ROS generation from LiCoO₂ indeed led
 59 to additional cellular oxidative injury. This study highlights the
 60 importance to characterize the dynamic variables independently in
 61 order to understanding the multiple paths that lead to oxidative
 62 stress responses in organisms.

Results and Discussion

Characterization of as-synthesized lithium cobalt oxide nanoparticles.

63 As-synthesized LiCoO₂ nanoparticles were characterize
 64 morphologically and structurally. Micrograph images from TEM show
 65 the typical morphology of these nano-structures (Fig 1) where a high
 66 magnification view of one of such structures shows the sheet-like
 67 morphology (Fig 1b). BET analysis yielded a surface value of 125 m²/g
 68 for the LiCoO₂ nanoparticles. The collected powder XRD pattern,
 69 published previously,²⁹ can be indexed to the R̄3m space group, as
 70 expected for this crystal structure. However, we note that the as-
 71 synthesized LiCoO₂ without the high temperature annealing step has
 72 lower crystallinity, which more-closely represents spent cathode
 73 materials after numerous electrochemical cycles, the condition at
 74 which environmental exposure occurs. Dynamic Light Scattering (DLS)
 75 measurements of 5 mg/L suspensions of particles in ultrapure
 76 water yielded diffusion coefficient and ζ -potential values of 0.8 ± 0.1
 77 $\mu\text{m}^2/\text{s}$ and -2.0 ± 1.0 mV, respectively. We report diffusion coefficient
 78 (in $\mu\text{m}^2/\text{s}$) of these particles as an indicator for size because it is a
 79 direct measurement from the DLS, while hydrodynamic diameter is
 80 calculated from diffusion coefficient assuming the particles to be
 81 spherical in shape, a poor assumption to make in this case.

LiCoO₂ dissolution and the release of cobalt ion over time.

82 Previously, both experimental^{25,30} and computational studies³¹ have
 83 demonstrated that LiCoO₂ nanoparticles can undergo partial
 84 dissolution in aqueous media. The extent and the kinetics of
 85 dissolution are dependent on nanomaterial surface properties,
 86 solution pHs and constituents. Prior studies^{10–12,25,26} examining the
 87 biological impact of this class of complex metal oxides with various
 88 model organisms have repeatedly indicated that the amount of Li⁺
 89 released, although significantly higher than those of the transition
 90 metal ions (e.g. Co²⁺, Ni²⁺ and Mn²⁺), has minimal impact to the

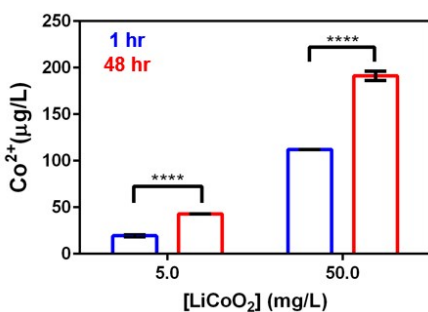


Figure 2. Co ion dissolution from LiCoO₂ upon suspension in bacterial growth minimal medium with 10 mM dextrose for 1 hr (blue) vs. 48 hrs (red) quantified by ICP-MS ($n = 3$, *** for $P < 0.0001$ with two-way ANOVA with Sidak's multiple comparison test). Error bars represent standard error of means.

organisms tested, *B. subtilis* included.¹¹ Therefore, we focus on the specific impact of cobalt ion released from the material in this study. ICP-MS analysis was used to quantify the time-dependent cobalt ion dissolution in the LiCoO₂ suspensions in a *B. subtilis* growth minimal medium. Fig 2 shows the amount of Co²⁺ released from 5.0 and 50.0 mg/L LiCoO₂ after suspension for 1-hr (blue) and 48-hr (red) periods. As expected, higher amounts of Co²⁺ ions were released in solution at the higher LiCoO₂ concentration, and as the nanoparticles were suspended for a longer period of time compared to a freshly suspended (1-hr) LiCoO₂ suspension.

LiCoO₂ generates abiotic ROS in growth medium.

In addition to ion release, previous investigations of complex metal oxides have revealed that, depending on the composition of the material, reactive oxygen species can be generated spontaneously upon material dissolution.²¹ ROS are known to cause oxidative stress resulting in cellular damage in bacteria.³² Therefore we aimed to first detect and identify if any ROS were generated simultaneously by LiCoO₂ nanoparticle suspensions in bacterial growth media.

Fig 3 shows the results from a selection of ROS probes used to detect and identify the presence of specific species in LiCoO₂ suspensions over time. Amplex Red™ assay,^{33,34} a horseradish peroxidase (HRP)-based assay that has been previously applied to detect H₂O₂ generated from TiO₂ nanoparticle suspensions³⁵ was used to detect and quantify H₂O₂ in LiCoO₂ NP suspensions. Fig 3a shows results from the quantification of H₂O₂ using Amplex Red, indicating the formation of abiotic ROS in bacterial growth medium with LiCoO₂ suspension, and the identity of the ROS is likely to be H₂O₂. Statistical analysis shows that the amounts of H₂O₂ generated from the freshly (1-hr) suspended LiCoO₂ NPs at both 5 and 50 mg/L level are significantly different from that of the control (blank medium), and the amounts of H₂O₂ detected in a 48-hr old suspension are significantly lower than those from freshly suspended LiCoO₂ at both concentrations ($P < 0.0001$, two-way ANOVA). The results suggest that ROS is indeed generated at an early stages of LiCoO₂ NP dissolution in aqueous media, yet the abiotic ROS signal decreases over time as the LiCoO₂ is left in solution for longer period of time.

Although the use of fluorescent probes is a common and effective approach to detecting ROS,³⁶ one of many possible errors that can

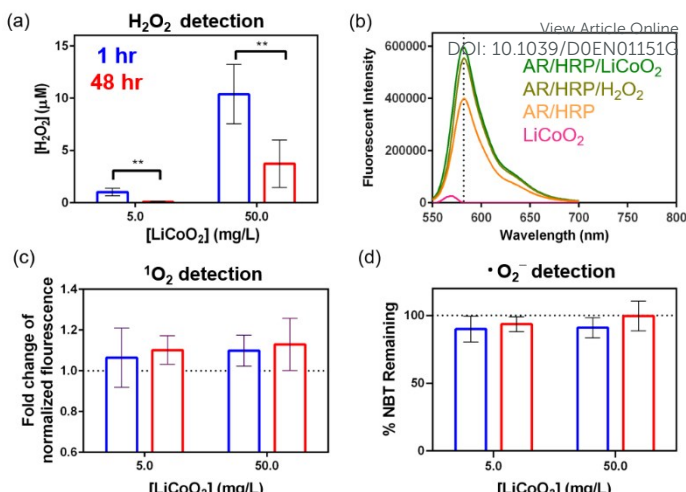


Figure 3. Abiotic ROS detection in LiCoO₂ suspension after 1-hr (blue) and 48-hr (red) in minimal media with 10 mM dextrose. (a) Quantification of hydrogen peroxide generated from LiCoO₂ suspensions monitored by Amplex Red dye ($n = 4$, ** for $P < 0.01$ with two-way ANOVA with Sidak's multiple comparison test), (b) Representative fluorescence spectra of 100 μM Amplex red (AR) and 0.1 unit·mL⁻¹ horseradish peroxidase (HRP) solution after 1 hr exposure through a filter membrane to LiCoO₂ nanoparticles and/or 1 μM H₂O₂ standard solution. (c) Normalized fluorescence signal from singlet oxygen sensor green (SOSG) for singlet oxygen detection. (d) Attenuation in absorbance at 259 nm of nitroblue tetrazolium solutions (NBT) upon exposure to LiCoO₂ solutions for superoxide generation detection.

arise when using such a probe molecule is false-positive detection via the probe reacting at a potentially catalytic surface, such as LiCoO₂ NPs.³⁷ To ensure that positive results of the Amplex Red assay were due to the transformation of Amplex Red to resorufin upon reaction with free H₂O₂ and not on the nanoparticle surfaces, we performed diffusion assays with LiCoO₂ suspension. We assembled an apparatus (Fig S1) to spatially separate the LiCoO₂ nanoparticles from the Amplex Red-HRP solution using a finely porous hydrophobic filter membrane. Fluorescence of the resulting solution above the filter membrane (*i.e.* no direct particle exposure) is used to detect H₂O₂ with 1 μM H₂O₂ below the filter membrane as a standard. Under this experimental design, an increase in fluorescence would be from the reaction of Amplex Red with free H₂O₂ and not with the nanoparticle surfaces, assuming i) H₂O₂ readily diffuses through the membrane, ii) LiCoO₂ cannot diffuse through the membrane (25 nm pores are small relative to particle diameter), and iii) HRP will not appreciably diffuse through the membrane within the time scale of the experiment. Although Amplex Red may diffuse through the membrane, conversion to the fluorescent product requires the HRP catalyst. Although we expect cobalt ions may also diffuse through the membrane, Co²⁺ alone did not induce fluorescence intensity change with Amplex Red in control experiment. Fig 3b shows representative fluorescence spectra of each sample tested with the normalized fluorescence intensity normalized to the background in the inset. The presence of LiCoO₂ NPs results in an increase in fluorescence compared to the AR-HRP control solution. Addition of 1 μM H₂O₂ spike produces a similar effect, indicating that H₂O₂ diffuses through the membrane over the 1 hr period and reacts with AR-HRP. The presence of LiCoO₂ particles alone (no AR-HRP) shows no fluorescence, with small background intensity coming from scattering of the excitation. These results show that positive

ARTICLE

1
2
3
4
5
6
7
8
9
10
11
12
13
14
15
16
17
18
19
20
21
22
23
24
25
26
27
28
29
30
31
32
33
34
35
36
37
38
39
40
41
42
43
44
45
46
47
48
49
50
51
52
53
54
55
56
57
58
59
60
detection of H_2O_2 in our Amplex Red experiment is indeed due to the presence of abiotic H_2O_2 and not direct interaction of Amplex Red with the $LiCoO_2$ NPs.

The singlet oxygen sensor green (SOSG) fluorescence dye was employed to discern the production of singlet oxygen in the $LiCoO_2$ dissolution and is highly specific to singlet oxygen detection. This dye manifests in weak blue color initially and emits green fluorescence with the presences of singlet oxygen (excitation/emission: 504/525 nm).¹⁹ Fig 3c shows that the normalized fluorescence signals indicating the $LiCoO_2$ suspension at different time points did not produce significant amount of singlet oxygen in solution when compared to control.

Lastly, the generation of superoxide was monitored by observing the reduction in absorbance at 259 nm of a nitro blue tetrazolium solution (NBT). Superoxide, if present, can react with NBT to form a precipitate, formazan, resulting in a decrease in the absorbance at 259 nm.³⁵ Fig 3d shows that the NBT absorbance signal does not decrease in the presence of $LiCoO_2$ suspension regardless of concentration and time-point, which suggests no superoxide formation by the $LiCoO_2$ nanoparticles in solution.

Results shown in Fig 3 overall confirms that ROS is generated by $LiCoO_2$ suspension in bacterial growth medium. More significantly, we were able to identify the species generated as hydrogen peroxide and quantify its concentrations in $LiCoO_2$ suspensions. The H_2O_2 diffusion experiment also critically illustrated that the observed fluorescence signal using a dye was not the results of optical interference by the nanomaterials, or by nanoparticle surface catalyzed chemical reaction of the dye molecules. The chemical nature of $LiCoO_2$ determines that cobalt is in the Co^{3+} state. In fact, we have detected a $Co(III)$ -EDTA complex spectroscopically when $LiCoO_2$ NP was dissolved in the presence of EDTA in solution (Fig S2). Upon dissolution, Co^{3+} is likely to reduce to the more soluble form of Co^{2+} . We have also observed the redox activity of $LiCoO_2$ upon suspension in aqueous media is able to oxidize the electron transporters, nicotinamide adenine dinucleotide (NADH) (unpublished). Therefore, we hypothesize that the $Co(III)$ reduction is then likely to trigger water oxidation and generate H_2O_2 .

Table 1. Comparison of $LiCoO_2$ nanoparticle properties at various stages of suspension in aqueous media.

	As-synthesized	Media-suspended 1-hr	Media-suspended 48-hr
z-potential (mV)	-2.0 ± 1.0	-28 ± 2	-25 ± 4
Diffusion coefficient ($\mu m^2/s$)	0.8 ± 0.1	0.9 ± 0.5	1.0 ± 0.2

Interestingly, by examining the solution constituents of the nanoparticle suspension at two different time points (1-hr vs. 48-hr), we were also able to probe the dynamic process of both ion release and ROS formation from complex metal oxides in aqueous medium. Although studies have indicated the importance to monitor ion

release from metal or metal oxide nanoparticles through dissolution over time because of ion-induced toxicity to organisms,^{10,11,36} there have been few studies examining abiotic ROS formation over time. We note that parallel attention is needed to monitor the generation of abiotic ROS in these nanoparticle suspensions over time as well as ion release, in order to develop a holistic view of the chemistry of material transformation.

On the other hand, the $LiCoO_2$ particles after suspension in media do not undergo noticeable changes morphologically compared to those freshly synthesized (Fig S3). The layered structure of the nanosheets remains visible. ζ -potential (ZP) analysis of medium-exposed $LiCoO_2$ also yielded comparable values as shown in Table 1. The exposed particles have more negative ZP values than that of the pristine particles, which is expected due to the surface-adsorbed phosphate species to $LiCoO_2$.³⁰ The diffusion coefficients of the medium-exposed particles after 1 hr and 48 hr exposure are also comparable with that of the pristine particles, suggesting minimal variations in particle size. This experimental evidence suggests that any transformations due to exposure to the medium is likely surface limited.

$LiCoO_2$ impacting bacterial viability

Previous studies have shown that transition metal oxides do not enter bacterial cells, in contrast to their interactions with eukaryote cells.^{10,25} Instead, the ions released from these materials often can recapitulate the impact on bacterial respiration^{10,11,38} and viability.³⁹ Therefore, we studied the effect of $LiCoO_2$ nanoparticles and the corresponding amount of ions released over time by monitoring the viability of *B. subtilis*. A growth-based viability (GBV) analysis was performed to quantify the relative amount of viable bacterial cells under different exposure conditions to $LiCoO_2$ nanoparticles by the periodic measurement of OD_{600} .⁴⁰ In this assay, the viability of bacterial cultures exposed to nanoparticles is assessed by comparing the delay in the culture regrown in fresh nutrient-rich media against a preconstructed calibration curve relating the delay to the number of viable cells. The assay is especially effective in evaluating nanotoxicity to bacterial species because it eliminates the concerns for nanomaterial aggregation in nutrient-rich media, and reduces optical interferences by nanomaterials in normal growth assays. We hypothesized that cobalt dissolution contributes significantly to the

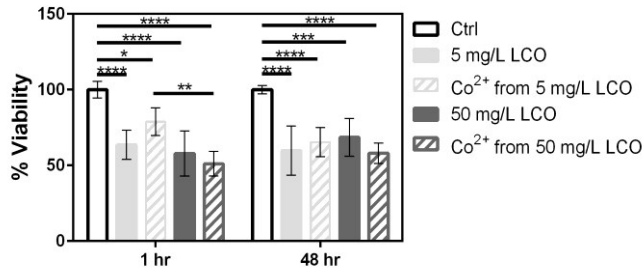


Figure 4. Bacterial viability of *B. subtilis* upon exposure to 5 and 50 mg/L of $LiCoO_2$ or their corresponding amount of Co^{2+} ion released at 1-hour and 48-hour time points (n = 4, one-way ANOVA with post-hoc Tukey's multiple comparisons test, * for p < 0.05, ** for p < 0.01, *** for p < 0.001 and **** for p < 0.0001).

impact of the bacterial population. Hence, viability comparisons were made between the LiCoO_2 suspensions and their corresponding amounts of dissolved cobalt ions at different time-points and concentrations. Fig 4 shows that at both time points and both concentrations examined, the bacterial viabilities have fallen to 50~70% compared to unexposed cells. The concentrations and the age of the LiCoO_2 suspension did not yield significant difference in the level of toxicity. Moreover, no significant differences in viability were observed induced by the LiCoO_2 and the cobalt ion released (solid vs. shaded bars) at each concentration and time point. In fact, when examining the bacterial viability as a function of LiCoO_2 (Fig S5a) and of Co^{2+} (Fig S5b) at wider concentration ranges, we observed that the correlation between the concentrations and viability is non-linear, which may explain the similarities in bacterial viability between the 5 and 50 mg/L LiCoO_2 treatments at various time points. Overall, the presence of LiCoO_2 and the released Co^{2+} both reduced viability of the bacterium. The released Co^{2+} recapitulate the impact of LiCoO_2 to *B. subtilis* viability at the concentrations and time points examined.

Bacterial intracellular ROS and oxidative stress responses induced by LiCoO_2

Cell viability and toxicity studies, although important indicators of the nanomaterial's impact, are often end-point measurements that do not provide detailed mechanistic insights of the more subtle biological changes. Hence, we examine the biological impact to LiCoO_2 by characterizing Co ion internalization and intracellular ROS generation guided by the observations of ion release (Fig 2) and the abiotic ROS generation (Fig 3). We first test the hypothesis that as the amount of Co^{2+} released in solution increases over time, a higher influx of Co^{2+} is internalized in bacterial cells. Therefore, the LiCoO_2 dissolution will likely result in increased metal ion influx in bacterial cells. Newport Green™ DCF is a cell permeable fluorescent dye used for the detection of divalent metal ion internalization in cells⁴¹ and has been previously successfully employed in bacterial species to monitor the internalization of divalent transition metal ions.^{39,42} Fig 5 shows an increase in fluorescence signal at increasing LiCoO_2 concentrations, revealing that, at both 5 and 50 mg/L of LiCoO_2 , there is a significant amount of Co^{2+} uptake in cells. Furthermore, significantly higher fluorescence signals were observed as the

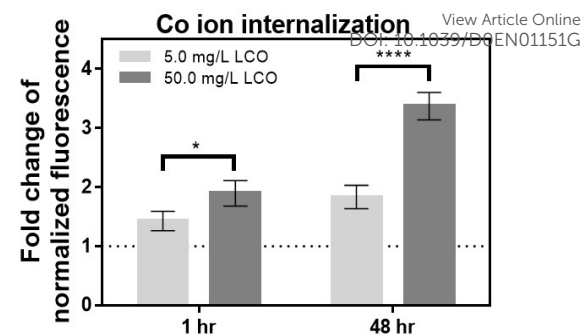


Figure 5. Normalized fluorescence signal from Newport Green™ dye for Co^{2+} ion internalization in *B. subtilis* upon exposure to 1-hour, and 48-hr old LiCoO_2 suspension in the minimal growth medium ($n = 4$, unpaired t -test with Welch's correction, * for $p < 0.05$, and **** for $p < 0.0001$).

LiCoO_2 CO suspension aged. This observation is consistent with the ICP-MS analysis (Fig. 2) which reported an increased cobalt ion release over time.

The detection of H_2O_2 in solution from LiCoO_2 suspension led us to examine the oxidative stress responses in bacterial cells. Intracellular ROS studies were conducted to understand how bacterial cells combat the oxidative stress upon exposure to LiCoO_2 . DCFH₂-DA, a generic ROS probe, was used for the detection of intracellular ROS in *B. subtilis* upon 30-min exposure to LiCoO_2 suspensions that were 1 hr- and 48 hr-aged (Fig 6a). Results show a clear increase in fluorescence signals from bacterial cells grown in media with increasing LiCoO_2 concentrations, which confirms the generation of intracellular ROS in *B. subtilis* under these exposure conditions. Similarly, intracellular ROS signals have been detected previously when trout gill cells were exposed to LiCoO_2 suspensions.²⁵ Interestingly, in contrast to the abiotic ROS signals from growth media (Fig 3a), intracellular ROS signals do not exhibit a time-dependent manner for LiCoO_2 NPs suspended for different durations (data replotted in Fig S6a for comparison) ($P > 0.05$ with two-way ANOVA). Although abiotic H_2O_2 is generated with an initial burst when freshly suspended, then decays at 48-hr, the intracellular ROS signals in bacteria remain rather constant. Therefore, it is critical to note that the biotic and abiotic ROS signals are generated through different mechanisms. Their correlation and interdependent nature will be discussed below.

Furthermore, in contrast to the lack of abiotic superoxide detected in solution (Fig 3d), Fig 6b shows fluorescence measurements from

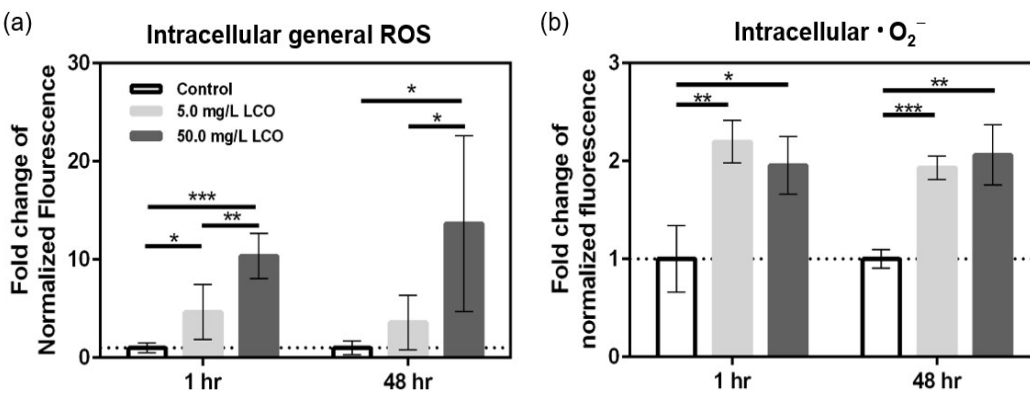


Figure 6. Intracellular ROS detection in *B. subtilis* grown in LiCoO_2 suspensions in minimal media with 10 mM dextrose. (a) Normalized fluorescence signal from DCF-DA dye, and (b) normalized fluorescence signal from Dihydroethidium (DHE) dye for intracellular superoxide in *B. subtilis* ($n = 6$, one-way ANOVA with Tukey's multiple comparisons test).

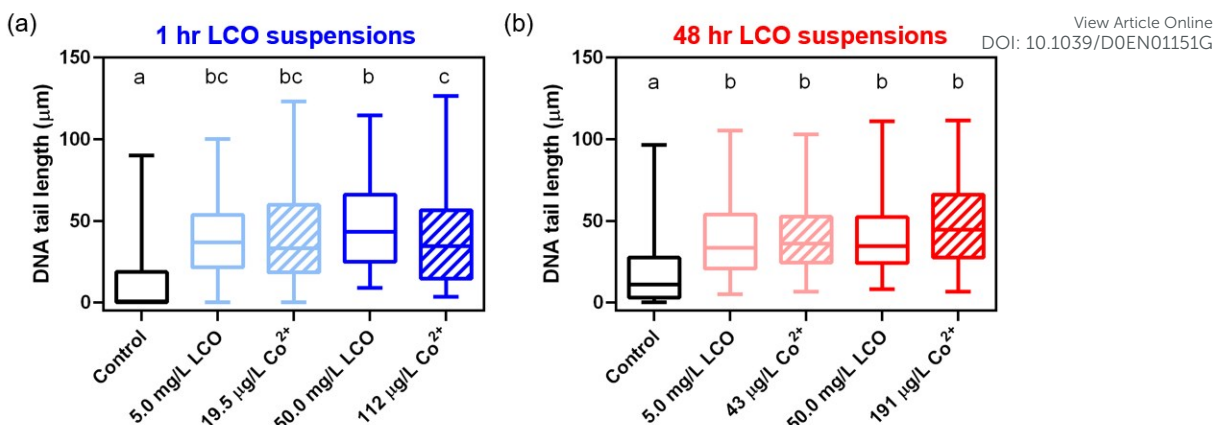


Figure 7. Comparison of bacterial DNA tail lengths resulted from single-cell gel electrophoresis analysis of *B. subtilis* upon exposure to (a) 1-hour, and (b) 48-hour LiCoO₂ NP suspensions. Shaded symbols represent treatments with equivalent amount of Co²⁺ released from LiCoO₂ NPs (n > 200; D'Agostino & Pearson normality test was first used to test for normal distribution; "a", "b", "c" denote statistically significant differences using the non-parametric Kruskal-Wallis tests with Dunn's multiple comparison).

the Dihydroethidium (DHE), a probe sensitive to detect intracellular superoxide,^{43,44} suggesting the generation of superoxide in *B. subtilis* grown in LiCoO₂ suspensions. Interestingly, the intracellular superoxide signals are neither concentration-dependent, nor LiCoO₂-suspension age-dependent (replotted in Fig S6b) ($P > 0.05$ with two-way ANOVA). In the intracellular environment, superoxide is often formed on the oxygen reduction pathway in a single-electron transfer redox reaction when molecular O₂ adventitiously oxidizes redox enzymes.^{45,46} Intracellular superoxide, once formed, can be further reduced to H₂O₂ in another one-electron redox process by superoxide dismutase, SOD.⁴⁵ Therefore, the generation and consumption of superoxide are likely to be a dynamic process in *B. subtilis*, which may explain the concentration- and suspension-age-independent behavior observed.

Because H₂O₂ can both permeate through the cell wall from LiCoO₂-containing media and be generated from intracellular superoxide reduction, we investigate the fate of intracellular H₂O₂ in *B. subtilis* using a luminescence dye, ROS-GloTM. Unfortunately, due to an optical interference of the dye in the presence of LiCoO₂ NPs, indicated by a color change upon mixing, we were unable to conduct the parallel experiment using LiCoO₂ NP-treated bacterial cells. Instead, we conducted experiments by dosing the bacterial culture with 30 μM H₂O₂ to observe the luminescence signals from cells upon treatment. The results from cells spiked with H₂O₂ distinctively show that H₂O₂ is not accumulated in bacterial cells, but is likely further converted (Fig S6). The intracellular concentration of H₂O₂ has been previously described as the difference between influx+intracellular formation and efflux+scavenging.⁴⁷ The diffusion rate of H₂O₂ across bacterial membrane can be matched by the rate of Alkyl hydroperoxide reductase (Ahp) or catalase turnover at the micromolar concentration levels of H₂O₂, which lowers intracellular H₂O₂ concentrations than that of the external environment.⁴⁸ Our results from ROS-GloTM indicate a dynamic and active conversion of H₂O₂ in *B. subtilis*.

LiCoO₂ induces bacterial DNA damage and changes in oxidative stress genes.

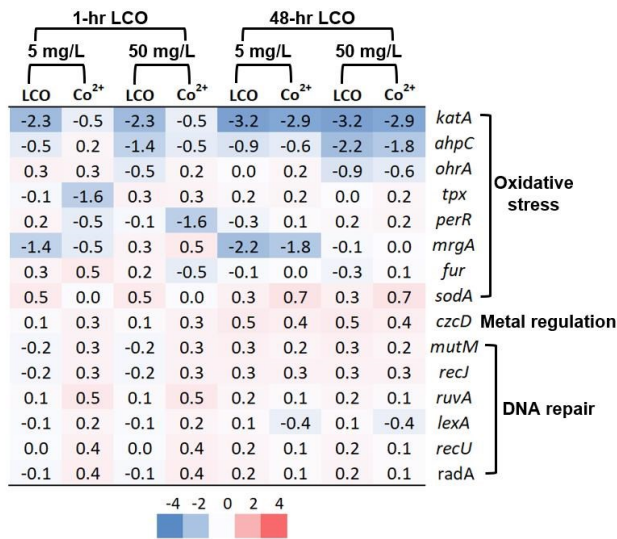
Intracellular H₂O₂ can either be converted to H₂O and O₂ by catalase, or react with labile Fe²⁺ in the intracellular environment through the

Fenton reaction to produce ·OH.^{34,48} Therefore, we further investigate the downstream biological impact of intracellular ROS. Although H₂O₂ does not normally damage DNA directly,⁴⁵ the highly transient and electrophilic ·OH is known to attack the electron-dense DNA molecules that lead to DNA damage.⁴⁹ Hence, although it is experimentally challenging to directly detect ·OH intracellularly, by monitoring the extent of bacterial DNA damage, we can probe the impact of this intracellular ROS. Single-cell gel electrophoresis (i.e., comet assay) at neutral pH environment is a sensitive method to detect and compare the extent of double-strand DNA breakage caused by exposure to LiCoO₂ NPs. The fragmented bacterial DNA exhibits a tail-like morphology upon nucleic acid staining, and the tail length is indicative of the extent of damage.^{50,51} We have previously used this method to assess the genotoxicity of nanomaterials to bacteria successfully.^{11,42}

Fig 7 shows the resulting DNA tail length analysis of *B. subtilis* upon exposure for 30 minutes to LiCoO₂ NP suspensions that are 1-hr (blue) or 48-hr (red) old, as well as the corresponding amounts of Co²⁺ released (shaded) at respective concentrations and time points. Because the DNA tail length is indicative of the extent of DNA damage, analysis of DNA tail length shows that both the LiCoO₂ NPs and Co²⁺ have induced significant DNA damage ($p < 0.0001$, non-parametric one-way ANOVA test). This observation suggests the presence of ·OH in *B. subtilis* upon exposure to both the LiCoO₂ NPs and Co²⁺.

Transition metals are well-known to induce oxidative stress through generating intracellular ROS.³⁴ Such properties of metal or metal oxide nanoparticles have also been explored as antibiotic agents towards bacterial species.⁵²⁻⁵⁴ Due to their multivalent nature, many transition metal ions can trigger redox chemistry in cellular environment by disrupting enzymatic functions and damaging biomolecules, such as proteins and DNA. In vitro studies have shown that Co²⁺ have been linked to single-strand breaks in salmon sperm DNA through Fenton-like reactions, and to create putative intrastrand cross-links of DNA.⁵⁵ Although Co(II) did not generate

Table 2. Heat map of changes in expression levels of selective genes related to oxidative stress, metal regulation, and DNA repair mechanisms in *B. subtilis* upon exposure to 1-hr and 48-hr LiCoO₂ suspensions and their corresponding amounts of Co ion released.



significant amount of ·OH when reacting with H₂O₂, a Co(I) mediated Fenton-like reaction has been proposed.⁵⁶ In addition, Co²⁺ can preferentially bind to specific sequences in DNA, e.g. the 5' G of GG sequences or the middle G of GGG.³⁴ We have also observed double-strand breakage induced by Ni²⁺ and Co²⁺,¹¹ as well as a variety of oxidative stress-related putative DNA adducts in two bacterial species upon exposure to nanoscale nickel manganese cobalt oxides in previous studies.⁴² Taken together, transition metal oxides generating multivalent metal ions that can enter bacterial cells and lead to bacterial DNA damage through Fenton-like reactions is likely a common toxicity mechanism for such materials.

Interestingly, when comparing the DNA tail lengths induced by LiCoO₂ NPs vs. the Co²⁺ alone, we observe different trends depending on the age of the LiCoO₂ suspensions. Fig 7a shows that, 50.0 mg/L freshly suspended (1-hr) LiCoO₂ NPs induced significantly longer DNA tails in comparison to those resulted from their dissolved Co²⁺ counterpart of 112 µg/L ($P < 0.05$, non-parametric ANOVA test with Dunn's multiple comparison test). Yet, no significant difference was observed in DNA tail length between LiCoO₂ NPs and their corresponding amount of dissolved Co²⁺ when the suspension is 48-hr old (Fig 7b). Together with solution H₂O₂ production in the 1-hr old LiCoO₂ NP suspensions that decayed over time (Fig 2a), we hypothesize that the increase in DNA tail length induced by fresh LiCoO₂ suspension may have resulted from the extracellular H₂O₂ generated in the fresh LiCoO₂ suspensions, which led to additional DNA damage that cannot be accounted for by the presence of Co²⁺ alone. H₂O₂, an uncharged species that can penetrate membranes⁴⁷ and enter bacterial cells, has been known to induce cellular stress whenever it is present in their extracellular habitat. With as little as 1 µM of intracellular H₂O₂, crippling levels of DNA damage has been reported in *E. coli*.⁴⁸

In addition to examine the resulting DNA damage in bacterial cells, gene expression changes related to bacterial oxidative stress, metal regulation and DNA repair mechanisms were also evaluated to help

understand the biological response to both LiCoO₂ NP suspensions and their corresponding amount of Co²⁺ released. The specific functions of each gene examined are included in Table S1 in the ESI. *B. subtilis* was exposed to fresh (1 hr) and aged (48 hr) suspensions of LiCoO₂ NPs and Co²⁺ at 5 and 50 mg/L concentration levels to complement the DNA damage analysis. The heat map in Table 2 shows that, among the three categories of genes examined, the ones related to oxidative stress pathways are most severely altered. None of the genes related to metal regulation or DNA repair is significantly changed compared to control.

In a previous global analysis of oxidative stress genes⁵⁷, it has been demonstrated that protection against H₂O₂ in *B. subtilis* was largely mediated by the induction of proteins controlled by the PerR regulon, representing the primary stress response. Among members of the PerR regulon, only *katA*, *mrgA*, and *zosA* can be strongly induced by the H₂O₂ treatment.^{58,59} Remarkably, *katA* and *mrgA*, encoding the vegetative catalase, KatA, and the metalloregulation DNA-binding stress protein, MrgA, respectively, are the most significantly altered genes in all testing conditions in our study. A previous study examining changes in the CAT gene in a benthic-dwelling organism, *C. riparius*, upon exposure up to 100 mg/L LiCoO₂ has also reported significant down regulation of the CAT genes.²⁶ In addition, *tpx*, another gene that is significantly changed in Fig 8a and 8b, encodes proteins that has been suggested to be a thiol peroxidase, has been linked to peroxide detoxification.⁵⁷

Fig 8 shows key comparisons of genes that were significantly changed upon exposure to LiCoO₂ and/or corresponding amount of Co²⁺ (see Fig S8 for plots including all genes). Interestingly, Fig 8a shows that 1-hr old LiCoO₂ NPs induced different levels of changes in the expressions of the *katA*, *mrgA* and *tpx* genes compared to Co²⁺ alone. Yet 48-hr aged LiCoO₂ NPs do not induce differences in gene expression levels when compared to Co²⁺ (Fig 8b). Cobalt exposure has been linked to negative impact on catalase expression in several multicellular organisms.^{26,60} Among bacterial species, Co-induced stress has been attributed to the disruption of heme synthesis and the ligand coordination in Fe-S protein clusters.^{52,61-64} More specifically, a study of Co-induced stress in *E. coli* has demonstrated that OxyR (a homologue to PerR in *B. subtilis*)-mediated responses were observed as a consequence of Fe-S homeostasis imbalance upon Co²⁺ exposure.⁶⁵ Therefore, the changes in gene expression levels upon Co²⁺ exposure in Fig 8 are expected in *B. subtilis*. However, the additional impact from freshly-suspended LiCoO₂ NP in Fig 8a suggest the presence of additional factors. We attribute that the observed differences are likely the results of H₂O₂ generated in fresh (1-hr) LiCoO₂ NP suspensions, which decreases over 48 hours. On the other hand, a greater concentration of Co²⁺ is released in the aged LiCoO₂ suspension, which may have contributed to the greater

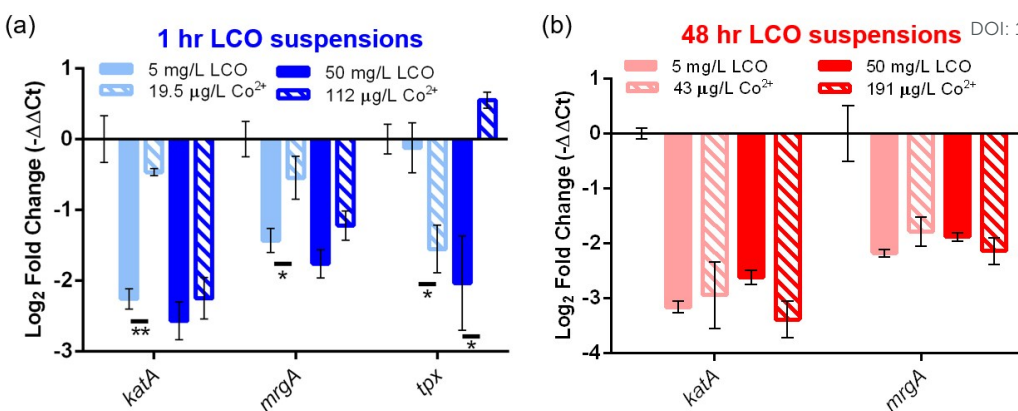


Figure 8. Comparisons of significantly changed genes in *B. subtilis* upon LiCoO₂ or Co²⁺ exposure. Solid bars refer to the response to LiCoO₂ NPs and striped bars represent the corresponding amount of Co ions. Error bars represent standard error of means (n = 4, ** for P < 0.01, and * for P < 0.05 according to one-way ANOVA with Tukey's multiple comparisons test).

impacts in these oxidative stress genes in the 48-hr old LiCoO₂ suspensions (Fig 8b). We also note that, interestingly, although we have observed an increase in intracellular O₂⁻ signals using a fluorescence probe (Fig 6a), no significant fold changes in the oxidative stress gene *sodA*, related to the superoxide anion, was observed. This difference could be due to the dynamic conversions of ROS in the intracellular environment. We note that the formation of intracellular superoxide from molecular oxygen could be catalyzed by Co²⁺,⁵⁶ and unlike H₂O₂, superoxide anion is not membrane permeant. The gene expression profile especially highlights the differences in cellular response to the stimulus of H₂O₂ (*katA*, *mrgA* and *tpx*), likely in response to the abiotic generation of H₂O₂ in the growth medium.

Oxidative stress in bacteria has been a well-reviewed area.^{32,45,48,66} It was recently proposed that induction of the OxyR regulon (PerR for *B. subtilis*) is one of the most reliable markers for oxidative stress in bacteria, as it is the bacterial detection system for intracellular H₂O₂.⁶⁶ We note that the connection between the generation of abiotic ROS in growth media and the intracellular ROS detected in model organism needs to be carefully established. Previous study has demonstrated that even when NPs do not generate abiotic ROS spontaneously, they may still induce intracellular ROS in mammalian cells and induce mitochondrial apoptosis.¹ Here, we demonstrate that the abiotic ROS (H₂O₂ in this case) generated in the process of NP transformation in solution can also trigger intracellular ROS and lead to additional oxidative stress responses in cells. Since both the abiotic ROS generation and intracellular ROS responses are dynamic, their correlation and interdependence can only be probed properly when both processes are monitored over time.

Conclusion

Altogether, our detailed analysis reveals that LiCoO₂ NPs in aqueous growth medium can spontaneously release cobalt ions and generate H₂O₂ when freshly suspended in solution. An initial burst of H₂O₂ in solution is followed by a subsequent decrease over time, while cobalt ion concentration increases over the time period monitored. Solution ROS generation from nanomaterials has previously been demonstrated largely in semiconductors and photosensitive

materials.^{1,3,19} LiCoO₂, as a model complex metal oxide, has not been previously identified as an ROS generator. The half reaction of LiCoO₂ reduction to generate Co²⁺ in water has a standard reduction potential of E⁰ = +2.14 V vs. SHE, which is likely to drive the oxidation half reaction of H₂O to form H₂O₂ (E⁰ = -1.76 V vs. SHE) thermodynamically. Therefore, it is critical to identify and quantify abiotic ROS formation, as well as to develop principles to predict biological impact upon NP exposure. We note that the fate of solution ROS, depending on its identity, can also be further influenced by media constituents, for instance pyruvate has been shown to sequester H₂O₂ to remediate cytotoxicity in mammalian cells,⁶⁷ and radical scavenger, Trolox, or serum proteins can mitigate lipid peroxidation by ROS generated from TiO₂ nanoparticles.⁶⁸

Overall, our study has revealed the intriguing dynamic oxidative stress responses in *B. subtilis* in response to the aqueous transformation of LiCoO₂. Although NP toxicity through dissolution and associated release of toxic ions into solution has been a well-established mechanism to organisms,^{18,69,70} the spontaneous formation of ROS in aqueous media by NPs coupled to ion release has been less investigated,^{1,3} especially in the absence of light or other energy sources. By using a bacterial model, and allowing the NP suspensions to transform independently from biological exposure, we successfully demonstrate the biological impacts of both ion release and the spontaneous formation of abiotic ROS by LiCoO₂. By acknowledging the dynamic nature of nanomaterial transformation which may trigger different subtle oxidative stress responses in organisms, we have designed the experiments that allow us to evaluate these variables independently. Although our attempt at tackling the dynamic process of nanomaterial transformation is coarse in this work (two time points), the information revealed provides us with insights into the subtle molecular-level responses in model organisms that have previously been obscured. Our approach is a crucial step towards a new way to evaluate nanotoxicity of complex metal oxides that will allow us to predict the environmental and biological impacts of these nanomaterials more accurately.

Materials and Methods

Journal Name

ARTICLE

Nanoparticle synthesis and transformation in bacterial growth medium

Synthesis of lithium cobalt oxide nanomaterials. We synthesized sheet-like nanoparticles of Li_xCoO_2 as described in detail in previous publications.^{29,30} Only a brief description is provided here. First Co(OH)_2 nanoparticles were prepared through a precipitation between lithium hydroxide, LiOH , and cobalt nitrate hexahydrate, $\text{Co}(\text{NO}_3)_2 \cdot 6\text{H}_2\text{O}$. The Co(OH)_2 precursor nanoparticles were then transformed into lithium cobalt oxide, Li_xCoO_2 by addition to a molten salt flux of $\text{LiNO}_3:\text{LiOH}$. The reaction in the molten salt flux was allowed to continue for 30 minutes, then quenched with water. The isolated precipitate was dried at 30 °C in a vacuum oven overnight, and stored in a glovebox under argon atmosphere when not in use.

Characterization of as-synthesized lithium cobalt oxide nanoparticles. Scanning electron micrographs of the pristine particles were taken using a Leo Supra55 VP scanning electron microscope, 3 kV electron energy, using a secondary electron detector. Nanoparticle surface area was analyzed by nitrogen physisorption Brunauer–Emmett–Teller (BET) analysis using a Micromeritics Gemini VII 2390 Surface Area Analyzer. Powder X-Ray Diffraction patterns were obtained using a Bruker D8 ADVANCE powder diffractometer with a $\text{Cu K}\alpha$ source and a Lynxeye detector. Dynamic light scattering (DLS) and zeta potential (ZP) measurements were taken using a Malvern Zetasizer Nano ZS. Transmission electron micrographs of fresh LiCoO_2 nanomaterial were obtained by dispersing 10 μL of a 1000x diluted stock LiCoO_2 suspension in Nanopure water on a Ted Pella copper grid with carbon type-B 300 mesh. The sample was then characterized on a JEOL 2100 Cryo TEM with LaB_6 emitter operated at 200 keV.

Lithium cobalt oxide nanoparticle transformation in growth medium. A minimal bacterial growth medium (11.6 mM NaCl , 4.0 mM KCl , 1.4 mM MgCl_2 , 2.8 mM Na_2SO_4 , 2.8 mM NH_4Cl , 88.1 μM Na_2HPO_4 , 50.5 μM CaCl_2 , 10 mM HEPES, and 10 mM dextrose) was used to represent a typical low nutrient natural environment and to reduce nanoparticle aggregation induced by proteins and amino acids. All experiments were conducted in this medium unless otherwise noted. Stock suspensions of LiCoO_2 in the growth medium for chemical transformation analysis were prepared at concentrations of 1000 mg/L by adding 2 mg of LiCoO_2 to 2 mL of medium. The suspensions were sonicated in a bath sonicator for 15 min and then incubated on a rotating plate at room temperature for either one hour (for “1-hr” LiCoO_2 samples) or 48 hours (for “48-hr” LiCoO_2 samples). After the incubation period, samples were diluted in the minimal medium to desirable concentrations for further analysis or bacterial exposure.

To quantify the cobalt ions released from the LiCoO_2 after aging, 5 and 50 mg/L diluted LiCoO_2 solutions prepared from the 1000 mg/L stock were centrifuged at 4000 $\times g$ for 10 min. A fraction of the supernatant was removed and ultra-centrifuged at 200,000 $\times g$ for 30 min. The supernatant was then removed to measure for cobalt ion content using the Inductively Coupled Plasma-Mass Spectrometry (ICP-MS), as done previously.³⁹

Abiotic ROS generation from lithium cobalt oxide nanoparticles

View Article Online

DOI: 10.1039/D0EN0115G

Solution hydrogen peroxide detection. To detect the formation of hydrogen peroxide, Amplex Red[®] reagent (Thermo Fisher) was used according to the manufacturer procedure. Amplex Red reagent and 0.2 U/mL Horseradish Peroxidase (HRP) were mixed with either standard hydrogen peroxide solutions, or LiCoO_2 suspensions at various concentrations to incubate in the dark at room temperature for 30 minutes.⁷¹ Fluorescence intensity was measured (535 nm / 590 nm) from a series of hydrogen peroxide standards to construct a calibration curve for the quantification of solution hydrogen peroxide generated in LiCoO_2 suspensions.

Solution singlet oxygen formation. The singlet oxygen sensor green (SOSG) (Thermo Fisher) can be used to detect the presence of singlet oxygen in solution by reacting specifically to singlet oxygen.¹⁹ LiCoO_2 suspension were mixed with the SOSG stock solution in a 0.1M HEPES buffer (pH 7.2). The generation of singlet oxygen was evaluated by measuring fluorescence at $\lambda_{\text{ex}} = 480$ nm and $\lambda_{\text{em}} = 528$ nm on a 96-well fluorescence plate reader. Fluorescence intensity was background corrected and normalized to those from control wells.

Solution superoxide detection. The formation of superoxide in LiCoO_2 suspension can be monitored by measuring the reduction of nitro blue tetrazolium (NBT).^{34,35} An NBT stock solution was mixed with LiCoO_2 suspensions and incubated at room temperature in the dark for 1 hour. The supernatant of the mixture was obtained through centrifugation (12,000 $\times g$, 5 min), and analyzed on a spectrophotometer at 259 nm. The formation of superoxide in solution is often indicated by the reduction in the peak intensity at 259 nm, resulted from the depletion of NBT upon reacting with superoxide.

Bacterial culture and lithium cobalt oxide nanoparticle exposure

Bacillus subtilis SB491 was purchased from the Bacillus Genetic Stock Center (Columbus, OH). Bacterial colonies were grown in solid lysogeny broth (LB) agar plates, and inoculated in LB growth medium overnight at 37 °C.

Lithium cobalt oxide nanoparticle toxicity to *B. subtilis*. Growth-based viability (GBV) was performed to assess the bacterial viability in the presence of aged LiCoO_2 .⁴⁰ *B. subtilis* was inoculated and grew in liquid LB at 37 °C overnight and harvested at mid-log phase. The cell pellets were then washed with Dulbecco phosphate-buffered saline (D-PBS) and resuspended in minimal medium with dextrose. The bacterial culture was then diluted to an $\text{OD}_{600\text{ nm}}$ of 0.05 with minimal medium. Bacterial culture at OD 0.05 was exposed to desired LiCoO_2 suspension conditions for 30 minutes while agitated, and reinoculated in fresh LB media for 16 hours. The growth curves were compared and analyzed to assess the impact of LiCoO_2 or Co^{2+} to bacterial viability.

Intracellular fluorescence assays

General intracellular ROS formation. To detect the formation of intracellular reactive oxygen species in general, the non-specific ROS fluorescence probe, 2',7'-dichlorodihydrofluorescein diacetate,

1 ARTICLE

2 DCFH₂-DA, was used according to manufacturer procedure. Bacterial
 3 cells were harvested at mid-log phase and adjusted to OD₆₀₀ of 0.2.
 4 DCFH₂-DA stock solution was added to the cell culture to a final dye
 5 concentration of 20 μ M, followed by an incubation at 37 °C for 1 hour
 6 in the dark. After incubation, cells pellets were resuspended in fresh
 7 minimal medium to eliminate the unreacted dye. LiCoO₂ suspensions
 8 were added to the dye-loaded cells and incubated with cells for 30
 9 minutes. Lastly, the LiCoO₂-treated bacterial culture were washed
 10 and resuspended in fresh minimal medium for OD₆₀₀ and
 11 fluorescence measurements (485 nm / 525 nm).

12
 13 **Dihydroethidium assay for intracellular superoxide.** To detect the
 14 formation of intracellular superoxide formation, Dihydroethidium
 15 (DHE) (Sigma Aldrich) was used.^{3,44} Bacterial cell cultures suspended
 16 in minimal medium with dextrose at OD₆₀₀ 0.6 were incubated with
 17 5 μ M DHE solution in the dark at 37 °C for 30 minutes. LiCoO₂
 18 suspensions at various concentrations were added to the dye-loaded
 19 cell cultures and incubated with cells for 30 minutes. Bacterial cell
 20 pellets were then centrifuged and resuspended in fresh minimal
 21 medium for OD₆₀₀ and fluorescence measurements (500 nm / 580
 22 nm).

23
 24 **Co²⁺ internalization in bacterial cells.** To monitor the internalization
 25 of Co²⁺, a DCFH₂-DA derivative dye, Newport Green™ (Thermo
 26 Fisher) was used.³⁹ Bacterial culture were adjusted to OD₆₀₀ 0.2 in
 27 minimal medium with dextrose, and incubated at 37 °C for 1 hour in
 28 the dark. After washing off the excessive dye and resuspending in
 29 fresh medium, the cells were exposed to LiCoO₂ suspension for 30
 30 minutes. After washing and resuspending in fresh medium, OD₆₀₀ and
 31 fluorescence intensity was recorded (505 nm / 535 nm).

32
 33 All intracellular fluorescence assays were first normalized over cell
 34 density (F/OD₆₀₀) to correct for any discrepancies in the number of
 35 bacterial cells. The corrected fluorescence intensities were then
 36 normalized over control to yield a “fold change”.

37
 38 **Bacterial DNA damage**

39
 40 Bacterial double-strand DNA breakage upon LiCoO₂ exposure as an
 41 indication for DNA damage has been studied using the single-cell gel
 42 electrophoresis method, as previously described.^{11,42} Briefly, 10 μ L of
 43 diluted LiCoO₂ exposed cells at OD₆₀₀ 0.05 were mixed in 100 μ L Low
 44 Melting Agar, and placed on a FLARE™ Slide (Trevigen, MD). Slides
 45 were incubated at 4 °C for 10 minutes to solidify, followed by the
 46 addition of a second LMA gel layer containing a 0.5 % lysozyme
 47 solution. Once the second layer is solidified, the slide was incubated
 48 at 37 °C for 30 minutes in the dark, followed by overnight immersion
 49 in a lysing solution (2.5 M NaCl, 100.0 mM EDTA, 10.0 mM Tris -HCl,
 50 1% sodium N-lauryl sarcosine, 0.6% Triton® X-100, pH 10.0), and an
 51 enzyme digestion solution (2.5 M NaCl, 10.0 mM EDTA, 10.0 mM Tris-
 52 HCl, and 0.5 mg/mL proteinase K, pH 7.4) at 37 °C for 2 hours. Slide
 53 then underwent electrophoresis in a chilled opaque electrophoresis
 54 tank with sodium acetate – Tris electrophoretic buffer at pH 9.0 at 12
 55 V for 30 minutes in the dark. The slide was then dehydrated in a
 56 sequence of solutions of 1 M ammonium acetate in ethanol (20
 57 minutes), absolute ethanol (30 minutes), and 70% ethanol (10
 58 minutes), and dried in ambient air for 5 minutes. Lastly, the slides
 59 were rehydrated in 20 μ L of DMSO solutions (5% DMSO, 10 mM
 60 Na₂HPO₄) and stained with 20 μ L of 1 μ M YOYO-1 dye in 5% DMSO
 61 and imaged with a fluorescence microscope (λ_{ex} = 491 nm, λ_{em} = 509
 62 nm). Positive controls have been previously conducted using
 63 kanamycin and a cationic polymer, poly(allylamine hydrochloride).

64
 65 **Changes in bacterial gene expression**

66
 67 To study the changes in gene expression levels in *B. subtilis* upon
 68 exposure to different age and concentrations of LiCoO₂ suspensions
 69 or to corresponding amount of Co²⁺ released, bacterial cultures were
 70 harvested at mid-log phase and adjusted to OD₆₀₀ of 0.2 in the
 71 minimal growth medium, and incubated with various nanoparticle or
 72 ion treatments at 37 °C for 30 minutes. After incubation, the exposed
 73 bacterial cells were harvested by spinning and flash-freezing, and
 74 stored in -80 °C until RNA extraction. Four biological replicates were
 75 collected for the controls and each treatment groups.

76
 77 A detailed description for RNA extraction is provided in the ESI. The
 78 same qPCR procedure has also been previously reported.⁴² Briefly, to
 79 synthesize complementary deoxyribonucleic acid (cDNA) following
 80 Invitrogen's protocols and the iCycler base module of an iQ5
 81 Multicolor Real-Time, extracted RNA was mixed with Master Mix 1
 82 (random primers (Invitrogen, 48190-011) and dNTP (Invitrogen,
 83 18427013)) for 5 minutes at 65 °C, then chilled on ice for 1 minute.
 84 Then Master mix 2 (5x- First Strand Buffer, Dithiothreitol,
 85 RNaseOUT™ recombinant ribonuclease inhibitors (Invitrogen,
 86 10777019), and Superscript RT III reverse transcriptase (Invitrogen,
 87 18080-044)) was added to the reaction in an iQ5 Multicolor Real-
 88 Time PCR Detection System at 25 °C for 5 minutes, 50 °C for 60
 89 minutes, 70 °C for 15 minutes for random primer extension. The
 90 resulting cDNA samples were characterized on a NanoDrop UV-vis
 91 spectrometer and stored at -20 °C until qPCR analysis.

92
 93 Target genes relevant to oxidative stress, metal homeostasis and
 94 DNA repair have been selected for *B. subtilis*. Table S1 in ESI provides
 95 detailed information regarding the functions of the genes and the
 96 sequences of the primers. For qPCR using an iQ5 real-time PCR
 97 detection system (Bio-Rad Laboratories) with SYBR Green for the
 98 fluorescent intercalating dye (iTaq™ Universal SYBR® Green
 99 Supermix, Bio-Rad), manufacturer protocol was followed. cDNA,
 100 primers and SYBR® Green Supermix (Bio-Rad) were combined to
 101 react in a qPCR 96-well plate. The reaction started at 95 °C for 10
 102 minutes to denature the DNA, followed by 40-times temperature
 103 cycles of amplification of 15 s at 95 °C and 30 s at 60 °C. The gene
 104 expression data was processed by normalizing the raw threshold
 105 cycle (C_t) numbers against the output of a housekeeping gene, *arsR*.
 106 Each qPCR reaction was duplicated, and each gene analysis included
 107 four biological replicates.

108
 109 **Statistical analysis**

110 Nanomaterial characterizations and quantitative analysis (e.g. ICP-
 111 MS) were carried out with three technical replicates and three
 112 analytical replicates. Biological exposure, intracellular ROS, viability,
 113 and gene expression experiments throughout the study were carried
 114 out at least in triplicates ($n \geq 3$). Depending on the parameters

Journal Name

compared in each analysis, different statistical tests were used. (6)
Details of the analysis are provided in each figure caption.

Bacterial cells used for single cell gel-electrophoresis analysis were from 4 biological replicates of nanoparticle or ion exposure. DNA tail length data from different replicates were deemed identical to be combined only when the tail lengths analysis from the control groups were not tested to be statistically different ($p > 0.05$). Merged DNA tail length data was tested for normality using the D'Agostino & Pearson normality test first, followed by non-parametric Kruskal-Wallis tests with Dunn's multiple comparisons test.

Conflicts of interest

There are no conflicts to declare.

Acknowledgements

This material is based upon work supported by the National Science Foundation under Grant No. CHE-2001611, the NSF Center for Sustainable Nanotechnology (CSN). The CSN is part of the Centers for Chemical Innovation Program. M.G. and P.L. acknowledge the generosity of Terry Lindstrom for The Lindstrom Family Research Fund through Augsburg University. E.D.L. is supported by the National Science Foundation Graduate Research Fellowship Program under grant no. DGE-1747503. Additional support to E.D.L. was also provided by the Graduate School and the Office of the Vice Chancellor for Research and Graduate Education at the University of Wisconsin-Madison with funding from the Wisconsin Alumni Research Foundation. The authors thank Michael P. Schwartz for helpful discussions. The authors gratefully acknowledge use of facilities and instrumentation supported by NSF through the University of Wisconsin Materials Research Science and Engineering Center (DMR-1720415).

Notes and references

(1) Xia, T.; Kovochich, M.; Brant, J.; Hotze, M.; Sempf, J.; Oberley, T.; Sioutas, C.; Yeh, J. I.; Wiesner, M. R.; Nel, A. E. Comparison of the Abilities of Ambient and Manufactured Nanoparticles to Induce Cellular Toxicity According to an Oxidative Stress Paradigm. *Nano Lett.* **2006**, *6*, 1794–1807.

(2) Serpone, N.; Emeline, A. V. Semiconductor Photocatalysis - Past, Present, and Future Outlook. *J. Phys. Chem. Lett.* **2012**, *3*, 673–677.

(3) Jayaram, D. T.; Kumar, A.; Kippner, L. E.; Ho, P.-Y.; Kemp, M. L.; Fan, Y.; Payne, C. K. TiO₂ Nanoparticles Generate Superoxide and Alter Gene Expression in Human Lung Cells. *RSC Adv.* **2019**, *9*, 25039–25047.

(4) Nel, A.; Xia, T.; Mädler, L.; Li, N. Toxic Potential of Materials at the Nanolevel. *Science* **2006**, *311*, 622–627.

(5) Nitta, N.; Wu, F.; Lee, J. T.; Yushin, G. Li-Ion Battery Materials: Present and Future. *Materials Today* **2015**, *18*, 252–264.

(14) Bayram, A. A.; Hussain, M. K.; Lee, S.; Kim, K.; Saha, S. K.; Yang, G. M.; Choi, H. Y.; Cho, S. G. The Role of Reactive Oxygen Species (ROS) in the Biological Activities of Metallic Nanoparticles. *Int. J. Mol. Sci.* **2017**, *18*, 1–21.

(15) Qiu, T. A.; Gallagher, M. J.; Hudson-Smith, N. V.; Wu, J.; Krause, M. O. P.; Fortner, J. D.; Haynes, C. L. Research Highlights: Unveiling the Mechanisms Underlying Nanoparticle-Induced ROS Generation and Oxidative Stress. *Environ. Sci. Nano* **2016**, *3*, 940–945.

(16) Qiu, T. A.; Clement, P. L.; Haynes, C. L. Linking Nanomaterial Properties to Biological Outcomes: Analytical Chemistry Challenges in Nanotoxicology for the next Decade. *Chem. Commun.* **2018**, *54*, 12787–12803.

(17) Nita, M.; Grzybowski, A. The Role of the Reactive Oxygen Species and Oxidative Stress in the Pathomechanism of the Age-Related Ocular Diseases and Other Pathologies of the Anterior and Posterior Eye Segments in Adults. *Oxid. Med. Cell. Longev.* **2016**, 3164734.

ARTICLE

(18) Xia, T.; Kovochich, M.; Liong, M.; Mädler, L.; Gilbert, B.; Shi, H.; Yeh, J. I.; Zink, J. I.; Nel, A. E. Comparison of the Mechanism of Toxicity of Zinc Oxide and Cerium Oxide Nanoparticles Based on Dissolution and Oxidative Stress Properties. *ACS Nano* **2008**, *2*, 2121–2134.

(19) Brunet, L.; Lyon, D. Y.; Hotze, E. M.; Alvarez, P. J. J.; Wiesner, M. R. Comparative Photoactivity and Antibacterial Properties of C60 Fullerenes and Titanium Dioxide Nanoparticles. *Environ. Sci. Technol.* **2009**, *43*, 4355–4360.

(20) Limbach, L. K.; Wick, P.; Manser, P.; Grass, R. N.; Bruinink, A.; Stark, W. J. Exposure of Engineered Nanoparticles to Human Lung Epithelial Cells: Influence of Chemical Composition and Catalytic Activity on Oxidative Stress. *Environ. Sci. Technol.* **2007**, *41*, 4158–4163.

(21) Gunsolus, I. L.; Hang, M. N.; Hudson-Smith, N. V.; Buchman, J. T.; Bennett, J. W.; Conroy, D.; Mason, S. E.; Hamers, R. J.; Haynes, C. L. Influence of Nickel Manganese Cobalt Oxide Nanoparticle Composition on Toxicity toward *Shewanella Oneidensis* MR-1: Redesigning for Reduced Biological Impact. *Environ. Sci. Nano* **2017**, *4*, 636–646.

(22) Horst, A. M.; Vukanti, R.; Priester, J. H.; Holden, P. A. An Assessment of Fluorescence- and Absorbance-Based Assays to Study Metal-Oxide Nanoparticle ROS Production and Effects on Bacterial Membranes. *Small* **2013**, *9*, 1753–1764.

(23) Schmidt, J.; Vogelsberger, W. Dissolution Kinetics of Titanium Dioxide Nanoparticles: The Observation of an Unusual Kinetic Size Effect. *J. Phys. Chem. B* **2006**, *110*, 3955–3963.

(24) Cui, Y.; Melby, E. S.; Mensch, A. C.; Laudadio, E. D.; Hang, M. N.; Dohnalkova, A.; Hu, D.; Hamers, R. J.; Orr, G. Quantitative Mapping of Oxidative Stress Response to Lithium Cobalt Oxide Nanoparticles in Single Cells Using Multiplexed *In Situ* Gene Expression Analysis. *Nano Lett.* **2019**, *19*, 1990–1997.

(25) Melby, E. S.; Cui, Y.; Borgatta, J.; Mensch, A. C.; Hang, M. N.; Chrisler, W. B.; Dohnalkova, A.; Van Gilder, J. M.; Alvarez, C. M.; Smith, J. N.; Hamers, R. J.; Orr, G. Impact of Lithiated Cobalt Oxide and Phosphate Nanoparticles on Rainbow Trout Gill Epithelial Cells. *Nanotoxicology* **2018**, *12*, 1166–1181.

(26) Niemuth, N. J.; Curtis, B. J.; Hang, M. N.; Gallagher, M. J.; Fairbrother, D. H.; Hamers, R. J.; Klaper, R. D. Next-Generation Complex Metal Oxide Nanomaterials Negatively Impact Growth and Development in the Benthic Invertebrate *Chironomus Riparius* upon Settling. *Environ. Sci. Technol.* **2019**, *53*, 3860–3870.

(27) Feng, Z. V.; Gunsolus, I. L.; Qiu, T. A.; Hurley, K. R.; Nyberg, L. H.; Frew, H.; Johnson, K. P.; Vartanian, A. M.; Jacob, L. M.; Lohse, S. E.; Torelli, M. D.; Hamers, R. J.; Murphy, C. J.; Haynes, C. L. Impacts of Gold Nanoparticle Charge and Ligand Type on Surface Binding and Toxicity to Gram-Negative and Gram-Positive Bacteria. *Chem. Sci.* **2015**, *6*, 5186–5196.

(28) Hang, M. N.; Hudson-Smith, N. V.; Clement, P. L.; Zhang, Y.; Wang, C.; Haynes, C. L.; Hamers, R. J. Influence of Nanoparticle Morphology on Ion Release and Biological Impact of Nickel Manganese Cobalt Oxide (NMC) Complex Oxide Nanomaterials. *ACS Appl. Nano Mater.* **2018**, *1*, 1721–1730.

(29) Laudadio, E. D.; Ilani-Kashkouli, P.; Green, C. M.; Kabengi, N. J.; Hamers, R. J. Interaction of Phosphate with Lithium Cobalt Oxide Nanoparticles: A Combined Spectroscopic and Calorimetric Study. *Langmuir* **2019**, *35*, 16640–16649.

(30) Laudadio, E. D.; Bennett, J. W.; Green, C. M.; Mason, S. E.; Hamers, R. J. Impact of Phosphate Adsorption on Complex Cobalt Oxide Nanoparticle Dispersibility in Aqueous Media. *Environ. Sci. Technol.* **2018**, *52*, 10186–10195.

(31) Abbaspour-Tamijani, A.; Bennett, J. W.; Jones, D. T.; Cartagena-Gonzalez, N.; Jones, Z. R.; Laudadio, E. D.; Hamers, R. J.; Santana, J. A.; Mason, S. E. DFT and Thermodynamics Calculations of Surface Cation Release in LiCoO₂. *Appl. Surf. Sci.* **2020**, *515*, 145865.

(32) Imlay, J. Diagnosing Oxidative Stress in Bacteria: Not as Easy as You Might Think. *Curr. Opin. Microbiol.* **2015**, *24*, 124–131.

(33) Grisham, M. B. Methods to Detect Hydrogen Peroxide in Living Cells: Possibilities and Pitfalls. *Comp. Biochem. Physiol. - A Mol. Integr. Physiol.* **2013**, *165*, 429–438.

(34) Angelé-Martínez, C.; Goodman, C.; Brumaghim, J. Metal-Mediated DNA Damage and Cell Death: Mechanisms, Detection Methods, and Cellular Consequences. *Metalomics* **2014**, *6*, 1358–1381.

(35) Jayaram, D. T.; Runa, S.; Kemp, M. L.; Payne, C. K. Nanoparticle-Induced Oxidation of Corona Proteins Initiates an Oxidative Stress Response in Cells. *Nanoscale* **2017**, *9*, 7595–7601.

(36) Fernández-Castro, P.; Vallejo, M.; San Román, M. F.; Ortiz, I. Insight on the Fundamentals of Advanced Oxidation Processes: Role and Review of the Determination Methods of Reactive Oxygen Species. *J. Chem. Technol. Biotechnol.* **2015**, *90*, 796–820.

(37) Bartosz, G. Use of Spectroscopic Probes for Detection of Reactive Oxygen Species. *Clinica Chimica Acta* **2006**, *368*, 53–76.

(38) Gunsolus, I. L.; Hang, M. N.; Hudson-Smith, N. V.; Buchman, J. T.; Bennett, J. W.; Conroy, D.; Mason, S. E.; Hamers, R. J.; Haynes, C. L. Influence of Nickel Manganese Cobalt Oxide Nanoparticle Composition on Toxicity toward *Shewanella Oneidensis* MR-1: Redesigning for Reduced Biological Impact. *Environ. Sci. Nano* **2017**, *4*, 636–646.

(39) Clement, P. L.; Kuether, J. E.; Borgatta, J. R.; Buchman, J. T.; Cahill, M. S.; Qiu, T. A.; Hamers, R. J.; Feng, Z. V.; Haynes, C. L. Cobalt Release from a Nanoscale Multiphase Lithiated

View Article Online
DOI: 10.1039/D0EN01151G

ARTICLE

Journal Name

1 Cobalt Phosphate Dominates Interaction with Shewanella
2 Oneidensis MR-1 and *Bacillus Subtilis* SB491. *Chem. Res.*
3 *Toxicol.* **2020**, *33*, 806–816.

4 (40) Qiu, T. A.; Nguyen, T. H. T.; Hudson-Smith, N. V.; Clement,
5 P. L.; Forester, D.-C.; Frew, H.; Hang, M. N.; Murphy, C. J.;
6 Hamers, R. J.; Feng, Z. V.; Haynes, C. L. Growth-Based
7 Bacterial Viability Assay for Interference-Free and High-
8 Throughput Toxicity Screening of Nanomaterials. *Anal.*
9 *Chem.* **2017**, *89*, 2057–2064.

10 (41) Zhao, J.; Bertoglio, B. A.; Devinney, M. J.; Dineley, K. E.;
11 Kay, A. R. The Interaction of Biological and Noxious
12 Transition Metals with the Zinc Probes FluoZin-3 and
13 Newport Green. *Anal. Biochem.* **2009**, *384*, 34–41.

14 (42) Qiu, T. A.; Guidolin, V.; Hoang, K. N. L.; Pho, T.; Carra', A.;
15 Villalta, P. W.; He, J.; Yao, X.; Hamers, R. J.; Balbo, S.; Feng,
16 Z. V.; Haynes, C. L. Nanoscale Battery Cathode Materials
17 Induce DNA Damage in Bacteria. *Chem. Sci.* **2020**, *11* (41),
18 11244–11258.

19 (43) F.; Stanicka, J.; Cotter, T. G. Recent Advances in Reactive
20 Oxygen Species Measurement in Biological Systems. *Trends*
21 *Biochem. Sci.* **2013**, *38*, 556–565.

22 (44) Dikalov, S. I.; Harrison, D. G. Methods for Detection of
23 Mitochondrial and Cellular Reactive Oxygen Species.
24 *Antioxidants and Redox Signaling.* **2014**, *20*, 372–382.

25 (45) Imlay, J. A. Pathways of Oxidative Damage. *Annu. Rev.*
26 *Microbiol.* **2003**, *57*, 395–418.

27 (46) Nogueira, V.; Hay, N. Molecular Pathways: Reactive Oxygen
28 Species Homeostasis in Cancer Cells and Implications for
29 Cancer Therapy. *Clin. Cancer Res.* **2013**, *19*, 4309–4314.

30 (47) Bienert, G. P.; Schjoerring, J. K.; Jahn, T. P. Membrane
31 Transport of Hydrogen Peroxide. *Biochim. Biophys. Acta -*
32 *Biomembr.* **2006**, *1758*, 994–1003.

33 (48) Imlay, J. A. Cellular Defenses against Superoxide and
34 Hydrogen Peroxide. *Annu. Rev. Biochem.* **2008**, *77*, 755–
35 776.

36 (49) Lloyd, D. R.; Carmichael, P. L.; Phillips, D. H. Comparison of
37 the Formation of 8-Hydroxy-2'-Deoxyguanosine and Single-
38 and Double-Strand Breaks in DNA Mediated by Fenton
39 Reactions. *Chem. Res. Toxicol.* **1998**, *11*, 420–427.

40 (50) Solanky, D.; Haydel, S. E. Adaptation of the Neutral
41 Bacterial Comet Assay to Assess Antimicrobial-Mediated
42 DNA Double-Strand Breaks in *Escherichia Coli*. *J. Microbiol.*
43 *Methods* **2012**, *91*, 257–261.

44 (51) Liao, W.; McNutt, M. A.; Zhu, W.-G. The Comet Assay: A
45 Sensitive Method for Detecting DNA Damage in Individual
46 Cells. *Methods* **2009**, *48*, 46–53.

47 (52) Lemire, J. A.; Harrison, J. J.; Turner, R. J. Antimicrobial
48 Activity of Metals: Mechanisms, Molecular Targets and
49 Applications. *Nat. Rev. Microbiol.* **2013**, *11*, 371–384.

50 (53) Giannousi, K.; Lafazanis, K.; Arvanitidis, J.; Pantazaki, A.;
51 Dendrinou-Samara, C. *View Article Online* *Hydrothermal Synthesis of Copper*
52 Based Nanoparticles: Antimicrobial Screening and
53 Interaction with DNA. *J. Inorg. Biochem.* **2014**, *133*, 24–32.

54 (54) Mitchell, S. L.; Carlson, E. E. Tiny Things with Enormous
55 Impact: Nanotechnology in the Fight Against Infectious
56 Disease. *ACS Infect. Dis.* **2018**, *4*, 1432–1435.

57 (55) Lloyd, D. R.; Phillips, D. H. Oxidative DNA Damage
58 Mediated by Copper(II), Iron(II) and Nickel(II) Fenton
59 Reactions: Evidence for Site-Specific Mechanisms in the
60 Formation of Double-Strand Breaks, 8-Hydroxydeoxyguanosine and Putative Intrastrand Cross-
61 Links. *Mutat. Res. - Fundam. Mol. Mech. Mutagen.* **1999**,
62 424, 23–36.

63 (56) Leonard, S.; Gannett, P. M.; Rojanasakul, Y.; Schwegler-
64 Berry, D.; Castranova, V.; Vallyathan, V.; Shi, X. Cobalt-
65 Mediated Generation of Reactive Oxygen Species and Its
66 Possible Mechanism. *J. Inorg. Biochem.* **1998**, *70*, 239–244.

67 (57) Mostertz, J.; Scharf, C.; Hecker, M.; Homuth, G.
68 Transcriptome and Proteome Analysis of *Bacillus Subtilis*
69 Gene Expression in Response to Superoxide and Peroxide
70 Stress. *Microbiology* **2004**, *150*, 497–512.

71 (58) Helmann, J. D.; Wu, M. F. W.; Gaballa, A.; Kobel, P. A.;
72 Morshedi, M. M.; Fawcett, P.; Paddon, C. The Global
73 Transcriptional Response of *Bacillus Subtilis* to Peroxide
74 Stress Is Coordinated by Three Transcription Factors. *J.*
75 *Bacteriol.* **2003**, *185*, 243–253.

76 (59) Fuangthong, M.; Herbig, A. F.; Bsat, N.; Helmann, J. D.
77 Regulation of the *Bacillus Subtilis* Fur and PerR Genes by
78 PerR: Not All Members of the PerR Regulon Are Peroxide
79 Inducible. *J. Bacteriol.* **2002**, *184*, 3276–3286.

80 (60) Kubrak, O. I.; Husak, V. V.; Rovenko, B. M.; Storey, J. M.;
81 Storey, K. B.; Lushchak, V. I. Cobalt-Induced Oxidative
82 Stress in Brain, Liver and Kidney of Goldfish *Carassius*
83 *Auratus*. *Chemosphere* **2011**, *85*, 983–989.

84 (61) Thorgersen, M. P.; Downs, D. M. Cobalt Targets Multiple
85 Metabolic Processes in *Salmonella Enterica*. *J. Bacteriol.*
86 **2007**, *189*, 7774–7781.

87 (62) Fantino, J. R.; Py, B.; Fontecave, M.; Barras, F. A Genetic
88 Analysis of the Response of *Escherichia Coli* to Cobalt
89 Stress. *Environ. Microbiol.* **2010**, *12*, 2846–2857.

90 (63) Ranquet, C.; Ollagnier-de-Choudens, S.; Loiseau, L.; Barras,
91 F.; Fontecave, M. Cobalt Stress in *Escherichia Coli*: The
92 Effect on the Iron-Sulfur Proteins. *J. Biol. Chem.* **2007**, *282*,
93 30442–30451.

94 (64) Majtan, T.; Frereman, F. E.; Kraus, J. P. Effect of Cobalt on
95 *Escherichia Coli* Metabolism and Metalloporphyrin
96 Formation. *BioMetals* **2011**, *24*, 335–347.

97 (65) Barras, F.; Fontecave, M. Cobalt Stress in *Escherichia Coli*
98 and *Salmonella Enterica*: Molecular Bases for Toxicity and
99 Resistance. *Metallomics* **2011**, *3*, 1130–1134.

ARTICLE

(66) Imlay, J. A. Where in the World Do Bacteria Experience Oxidative Stress? *Environ. Microbiol.* **2019**, *21*, 521–530.

(67) Kelts, J. L.; Cali, J. J.; Duellman, S. J.; Shultz, J. Altered Cytotoxicity of ROS-Inducing Compounds by Sodium Pyruvate in Cell Culture Medium Depends on the Location of ROS Generation. *Springerplus* **2015**, *4*, 269.

(68) Runa, S.; Khanal, D.; Kemp, M. L.; Payne, C. K. TiO₂ Nanoparticles Alter the Expression of Peroxiredoxin Antioxidant Genes. *J. Phys. Chem. C* **2016**, *120*, 20736–20742.

(69) Dekkers, S.; Williams, T. D.; Zhang, J.; Zhou, J.; Vandebril, R. J.; De La Fonteyne, L. J. J.; Gremmer, E. R.; He, S.; Guggenheim, E. J.; Lynch, I.; Cassee, F. R.; De Jong, W. H.; Viant, M. R. Multi-Omics Approaches Confirm Metal Ions Mediate the Main Toxicological Pathways of Metal-Bearing Nanoparticles in Lung Epithelial A549 Cells. *Environ. Sci. Nano* **2018**, *5*, 1506–1517.

(70) Schultz, A. G.; Boyle, D.; Chamot, D.; Ong, K. J.; Wilkinson, K. J.; McGeer, J. C.; Sunahara, G.; Goss, G. G. Aquatic Toxicity of Manufactured Nanomaterials: Challenges and Recommendations for Future Toxicity Testing. *Environ. Chem.* **2014**, *11*, 207–226.

(71) Zhao, B., Summers F. A, and Mason, R. P. Photooxidation of Amplex Red to Resorufin: Implications of Exposing the Amplex Red Assay to Light. *Free Radic. Biol. Med.* **2012**, *53*, 1080–1087

View Article Online
DOI: 10.1039/D0EN01151G